Grid Integration of Offshore Wind Farms Using Modular Marx Multilevel Converters

Luís Encarnação[1], José Fernando Silva[2], Sónia F. Pinto[2], and Luis M. Redondo[1]

[1] Instituto Superior de Engenharia de Lisboa, Cie3, Portugal
{luisrocha,lmredondo}@deea.isel.pt
[2] Instituto Superior Técnico, Cie3, TU Lisbon, Portugal
fernandos@alfa.ist.utl.pt, soniafp@ist.utl.pt

Abstract. This paper proposes the use of a Modular Marx Multilevel Converter, as a solution for energy integration between an offshore Wind Farm and the power grid network. The Marx modular multilevel converter is based on the Marx generator, and solves two typical problems in this type of multilevel topologies: modularity and dc capacitor voltage balancing. This paper details the strategy for dc capacitor voltage equalization. The dynamic models of the converter and power grid are presented in order to design the converter ac output voltages and the dc capacitor voltage controller. The average current control is presented and used for power flow control, harmonics and reactive power compensation. Simulation results are presented in order to show the effectiveness of the proposed M^3C topology.

Keywords: modular multilevel converter, offshore wind farm, dc capacitor voltage equalization.

1 Introduction

The multilevel conversion of electric energy is appropriate for high levels of voltage and current, and therefore suitable for power and energy systems applications. The technology for the energy transmission system between wind farm and onshore grid can be done using ac connection (High Voltage Alternating Current - HVAC) or dc connection (High Voltage Direct Current - HVDC) [1]. This paper uses dc connection (HVDC - VSC voltage source converter) and proposes a three-phase modular multilevel Marx converter ($3M^3C$), with five levels for each phase leg, to connect the dc wind farm to the inshore power electrical network. The modular multilevel converter is based on the Marx generator (M^3C) [2,3,4] and solves two typical problems with known multilevel converter topologies [5,6], such as the Neutral-Point Clamped (NPC) and flying capacitor (FC). These topologies are non modular being difficult to balance the dc capacitor voltages, for topologies with levels higher than three. The five-level multilevel converter leg topology uses 8 basic cells for each arm (4 cells for each half arm). The three-phase 5 level multilevel converter uses 24 basic cells (3×8), and each basic cell has a capacitor which will be charged with $U_{Ci}=U_{dc}/(n-1)$, where n represents the number of levels (in this case $n=5$, implying $U_{Ci}=U_{dc}/4$).

Section 2 presents the technological contribution of this paper to value creation. In Section 3, the $3M^3C$ with five levels for each phase leg is presented. The dynamic models of the converter and power grid are presented in Section 4, in order to obtain the converter ac output voltages for a linear three-phase inductive load, and the dc capacitor voltage controller. The average current control [7,8] is presented and used for power flow control, harmonics and reactive power compensation. A sigma-delta modulator is applied to a M^3C leg, and a sliding-mode approach [9] is used to enforce the converter ac output voltages. The strategy for dc capacitor voltage equalization is presented with a detailed implementation of the algorithm. Simulation results are presented in Section 5 to show the effectiveness of the proposed solution.

2   Contribution to Value Creation

This paper proposes a solution for energy integration between an offshore Wind Farm and the power grid network, using a three-phase M^3C with five levels for each converter arm. The solution presented enables cleaner electrical energy because it uses controllers to reactive power and harmonic compensation. This work will contribute to value creation as it also allows a better use of renewable energy and the development of new technologies to enhance economic activity, creating more labor, more jobs while showing the potential to reduce; 1) the price per kilowatt, 2) the costs of imported fossil fuels and 3) the carbon dioxide emissions.

3   Three-Phase Modular Multilevel Marx Converter $3M^3C$

Three-phase modular multilevel Marx converter ($3M^3C$) with five levels for each leg is described. The proposed modular converter is based on Marx generators and uses M^3C topology (Fig. 1a). Its operation is described in detail in [2]. This topology has three bi-directional switches (S_k D_k, S_{ka} D_{ka} and $S_{k\,k+1}$ $D_{k\,k+1}$) and a capacitor denoted C_k that will be charged with $U_{Ck}=U_{dc}/(n-1)$, where $n=5$, implying $U_{Ck}=U_{dc}/4$, and k represents the number of M^3C cells or modules. The strategy to equalize all C_k capacitors will be explained in Section 4.4.

With the basic M^3C cell, n levels MCs can be obtained, using n-1 basic cells for the upper arm, and n-1 cells for the bottom arm. The five-level MC leg topology uses four basic cells (Fig. 1b) for each half arm, with a total of 8 cells for each converter arm (or phase). A three-phase $3M^3C$ with five levels for each phase uses twenty four basic cells (Fig. 1b). To understand the operating principles of three-phase M^3C, consider the five-level leg in which, to verify Kirchhoff's laws, (n-1) basic cells must present the voltage $U_{dc}/(n-1)$. Table 1 show all possible combinations with the basic cells (bottom and top arm) to have 4 basic cells turned off (S_{Ka} on) and 4 turned on (S_K on) and the corresponding voltage levels on each arm.

Table 1 shows the five voltage levels of voltage U_{Load} and the number of vectors for each level (there are 36 redundant vectors in level 3).
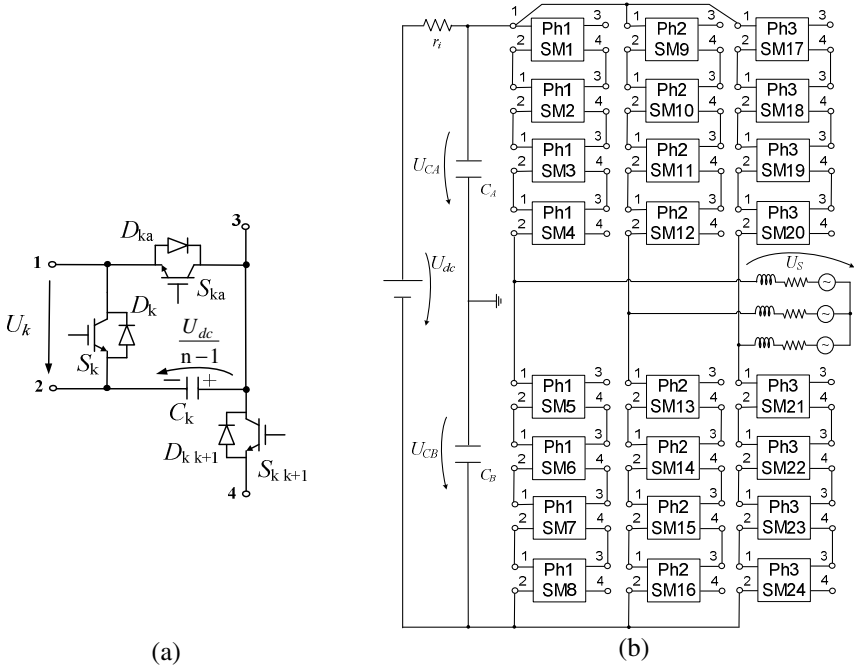
Fig. 1. Modular Multilevel Marx Converter topology: a) Structure of the basic cell; b) Three-phase M^3C with five levels for each phase leg (Ph→phase SM→sub-module cell)

Table 1. Voltage levels and number of vectors for a Five-Level M^3C leg

Level	U_{Load}	Number of ON Cells		Number of Vectors
		Upper	Bottom	
1	$-U_{dc}/2$	0	4	1×1=**1**
2	$-U_{dc}/4$	1	3	4×4=**16**
3	0	2	2	6×6=**36**
4	$+U_{dc}/4$	3	1	4×4=**16**
5	$+U_{dc}/2$	4	0	1×1=**1**

4 Modeling and Controller Design of M^3C Connection to Inshore Network

The dynamic models of the dc offshore fed M^3C to the inshore ac network are obtained in this section, together with the average current control used for power flow, harmonic and reactive power compensation. The strategy to equalize all the capacitors voltages is presented with a detailed implementation of the *Vector Decision* algorithm.
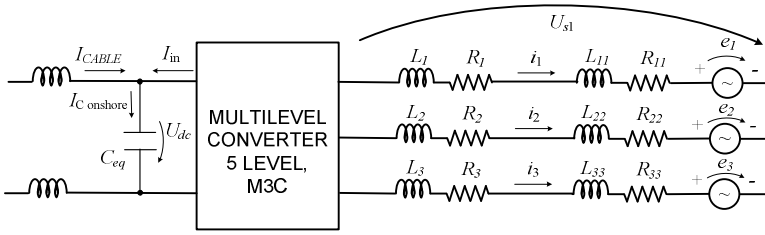
Fig. 2. Electrical diagram of offshore dc fed M³C to the inshore ac network

4.1   Modeling the M³C Connection to Inshore AC Network

The ac side model (Fig. **2**) in system coordinates (123) can be obtained using the *Kirchhoff* voltage and current laws, considering $R_1=R_2=R_3$ and $R_{11}=R_{22}=R_{33}$ and $L_1=L_2=L_3$ and $L_{11}=L_{22}=L_{33}$ then $R_{eq}=R_1+R_{11}$ and $L_{eq}=L_1+L_{11}$:

$$\begin{cases} U_{S1} = R_{eq}\,i_1 + L_{eq}\dfrac{di_1}{dt} + e_1 \\[2mm] U_{S2} = R_{eq}\,i_2 + L_{eq}\dfrac{di_2}{dt} + e_2 \\[2mm] U_{S3} = R_{eq}\,i_3 + L_{eq}\dfrac{di_3}{dt} + e_3 \end{cases} \tag{1}$$

The system model in dq0 coordinates (2) can be obtained applying *Park's* transformation to (1). The average current control method uses this state-space model (2) for power flow control, harmonics and reactive power compensation.

$$\begin{cases} \dfrac{di_d}{dt} = -\dfrac{R_{eq}}{L_{eq}}i_d + \dfrac{1}{L_{eq}}\left(L_{eq}\omega\,i_q + u_d - e_d\right) \\[2mm] \dfrac{di_q}{dt} = -\dfrac{R_{eq}}{L_{eq}}i_q + \dfrac{1}{L_{eq}}\left(-L_{eq}\omega\,i_d + u_q - e_q\right) \end{cases} \tag{2}$$

4.2   Linear Control of the U_{dc} Voltage

This section presents the dc capacitor voltage controller (Fig. 1b). The linear control of the U_{dc} voltage provides the $i_{d\,ref}$ component which in turn will be used to enforce the converter ac output voltages references. The controller is designed from the converter model (dc side) in dq0 coordinates (Fig. 3).

Considering $Ceq = \dfrac{C_A}{2} = \dfrac{C_B}{2} = \dfrac{C}{2}$ and $U_{CA} = U_{CB} = \dfrac{U_{dc}}{2}$ the equivalent model of the converter and offshore farm is shown in Fig. 3, and from the circuit depicted the U_{dc} voltage dynamics is:

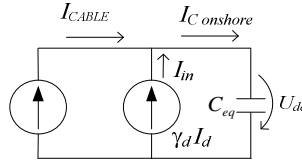$$C_{eq}\,\frac{dU_{dc}}{dt} = I_{CABLE} + \gamma_d I_d \tag{3}$$

Fig. 3. Equivalent model of the converter DC side

Neglecting the pole associated to a small time delay T_d in the current controlled current source $\gamma_d I_d$, the block diagram for the U_{dc} control is shown in Fig. 4.
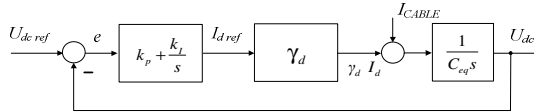

Fig. 4. Block diagram of the linear control of the U_{dc} voltage

The transfer function results in a 2nd order system (4) with a zero located in $-k_I/k_P$.

$$\frac{U_{dc}(s)}{U_{dc\,ref}(s)} = \frac{\dfrac{k_P\,\gamma_d}{C_{eq}}\,s + \dfrac{k_I\,\gamma_d}{C_{eq}}}{s^2 + \dfrac{k_P\,\gamma_d}{C_{eq}}\,s + \dfrac{k_I\,\gamma_d}{C_{eq}}} \tag{4}$$

In order to obtain a fast response with reduced overshoot, the zero of the controller should obey $-k_I/k_P \leq -\xi\omega_n$, therefore the $C(s)$ controller is designed for a damping factor $\xi = \sqrt{2}/2$ and $\omega_n = 2\pi\times25$ rad.s^{-1} ($\omega_n \ll 2\pi/T_d$), the following relations hold:

$$\begin{cases} 2\xi\omega_n = \dfrac{k_P\,\gamma_d}{C_{eq}} \\ \omega_n^2 = \dfrac{k_I\,\gamma_d}{C_{eq}} \end{cases} \Rightarrow \begin{cases} k_P = \dfrac{2\xi\omega_n C_{eq}}{\gamma_d} \\ k_I = \dfrac{\omega_n^2\,C_{eq}}{\gamma_d} \end{cases} \tag{5}$$

Using the M^{3}C converter parameters, $C_{eq} = 2$ mF ; $\gamma_d = \dfrac{u_d}{U_{dc}} = \dfrac{100\text{kV}}{200\text{kV}} = 0.5$ the PI parameters are k_I=98.7 and k_P=0.9.

4.3   Linear Control of i_d and i_q Currents

This section details the average current control of i_d and i_q currents. From the state-space model (2) in dq0 coordinates, making $H_d = L_{eq}\omega i_q + u_d - e_d$ and $H_q = -L_{eq}\omega i_d + u_q - e_q$ the linear model (**6**) is obtained. To obtain the control value H_d we use a PI controller where I_{dref} (set-point) is obtained from the output of the U_{dc} voltage controller. To obtain H_q another PI controller is used, with the set-point I_{qref}=0 to ensure reactive power compensation and harmonics mitigation.

$$\begin{cases} \dfrac{di_d}{dt} = -\dfrac{R_{eq}}{L_{eq}} i_d + \dfrac{H_d}{L_{eq}} \\[2ex] \dfrac{di_q}{dt} = -\dfrac{R_{eq}}{L_{eq}} i_q + \dfrac{H_q}{L_{eq}} \end{cases} \tag{6}$$

Neglecting R_{eq} the following block diagram was obtained (Fig. 5):
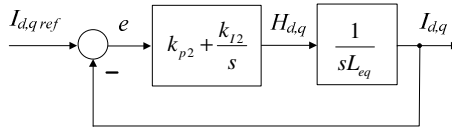
Fig. 5. Block diagram of the linear control of I_d

The resulting 2nd order system with a zero enables the calculation of k_{P2} and k_{I2}:

$$\begin{cases} 2\xi_2 \omega_{n2} = \dfrac{k_{P2}}{L_{eq}} \\[2ex] \omega_{n2}{}^2 = \dfrac{k_{I2}}{L_{eq}} \end{cases} \Rightarrow \begin{cases} k_{P2} = 2\xi_2 \omega_{n2} L_{eq} \\[1ex] k_{I2} = \omega_{n2}{}^2 L_{eq} \end{cases} \tag{7}$$

The PI controllers are also designed for a damping factor $\xi_2 = \sqrt{2}/2$ and $\omega_{n2}=2\pi\times25$ rad.s^{-1}. Considering $L_{eq}=L_1+L_{11}=32$mH (

Fig. **2**), the PI parameters are k_{I2}=789.6 and k_{P2}=7.1. Equations of H_d and H_q can be solved for u_d and u_q to obtain the ac output voltages (Fig. 6).
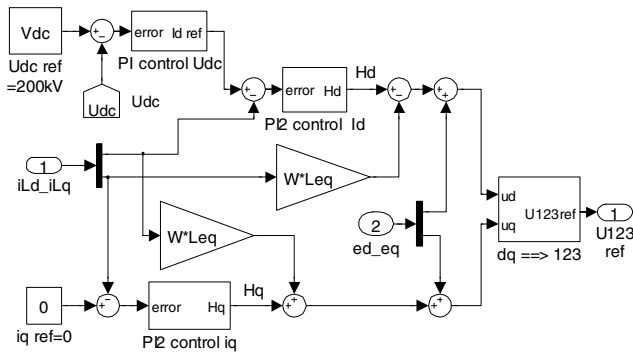
Fig. 6. Block diagram with average current control method to obtain the converter ac output voltages

Using inverse Park transformation three sinusoidal voltages references can be obtained from u_d and u_q. Then these voltages are fed to three sigma-delta modulators to obtain the three converter ac output voltages in phase coordinates (Fig. 7). Each sigma-delta modulator uses the sliding-mode stability condition to ensure the desired

voltage applied to the load by increasing or decreasing the chosen level. The modulator uses five levels, u_{mk} ($\pm\frac{1}{2}$ U_{dc}=100kV, $\pm1/4$ U_{dc}=50kV and 0V) to obtain the voltage output U_1.
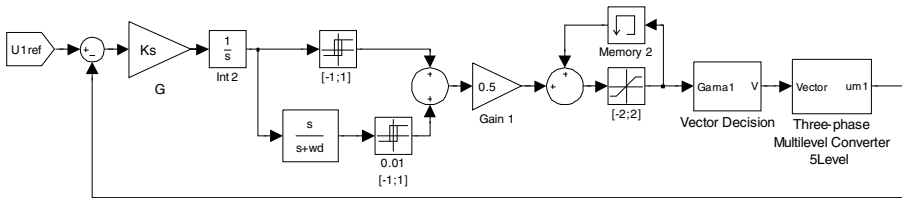

Fig. 7. Block diagram of sigma-delta modulator to obtain the converter ac output voltages

4.4   DC Capacitor Voltage Balancing

To balance all the capacitor voltages a *Vector Decision* algorithm was developed. This algorithm does not need data from the capacitor voltage measurements.

For three-level MC leg topology the algorithm is not necessary to balance the capacitors voltages, because the $S_{k\ k+1}$ semiconductor of each basic cell (Fig. 1a) guarantees voltage balancing. However, for M^3C with leg levels higher than three, a different strategy is needed. The idea of the *Vector decision* algorithm is to equally select the n-1 vectors of each intermediate level (2, 3 and 4), where n represents the number of levels. To obtain the first (-U_{dc}/2) and the fifth voltage level (+U_{dc}/2), only one vector is available. Therefore, the control of each converter leg will use 14 vectors (1+4+4+4+1) (Table 2). The *Vector decision* algorithm must use different cells (turned on) in the same level to perform capacitor voltage balancing. Since in the intermediate levels there are (3×4) redundant vectors a counter for each leg was devised as a function of the respective level (Table 2). The redundant vectors produce the same output voltage in the converter but different effects in the capacitors (charge or discharge). Table 2 shows the redundant vector choice (a, b, c, d) in states -1, 0, 1 to guarantee capacitor voltage balance.

The algorithm assigns a different vector for each leg as defined in table 2. The decision vector is chosen from the output status C_k and the output of the sigma delta modulator, γ_k value. Each C_k output depends on the status of three internal counters, one for each intermediate level ($C_{10}\Leftrightarrow\gamma_{-1}$, $C_{20}\Leftrightarrow\gamma_0$, $C_{30}\Leftrightarrow\gamma_1$). This internals counters, reset to one after three increments, repeating the same sequential assignment for each cycle.

Table 2. Vector decision Table

C_k \ γ_k	-2	-1	0	1	2
0	V1				V5
1		V2a	V3a	V4a	
2		V2b	V3b	V4b	
3		V2c	V3c	V4c	
4		V2d	V3d	V4d	

5   Simulation Results

The grid integration of an offshore wind farm using a modular Marx multilevel converter was simulated using MATLAB/Simulink environment in accordance with Fig. 8. These simulations illustrates the three-phase M^3C operating as a multilevel inverter to deliver energy (3 sinusoidal output voltages with reference amplitude equal to 100kV) from the offshore wind park (bipolar connection) to the power grid. The main circuit parameters (Fig. 1, Fig. **2** and Fig. 8) are U_{dc}=200kV, C_A=C_B=4mF, 24 Capacitor cell C_{1-24}=400μF, R_1=0.33Ω, L_1=30mH, R_{11}=0.1Ω, L_{11}=2mH.
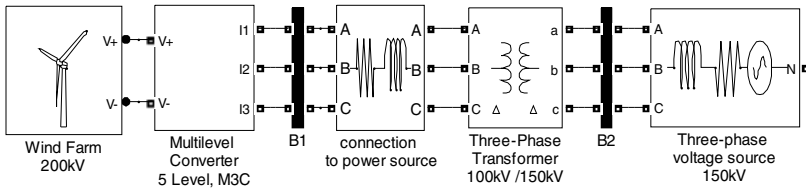

Fig. 8. Block diagram of the dc fed M^3C Connection to Inshore ac Network

In order to verify the effectiveness of the proposed strategy power variations were simulated from offshore wind park (begin with 500A, then change to 700A at 0.4s, and after to 800A at 0.6s and finally a step current to 1000A at 0.8s. Fig. 9 shows the 8 capacitor voltages in arm 1 balanced within approximately ±5% of their working voltage (50kV).
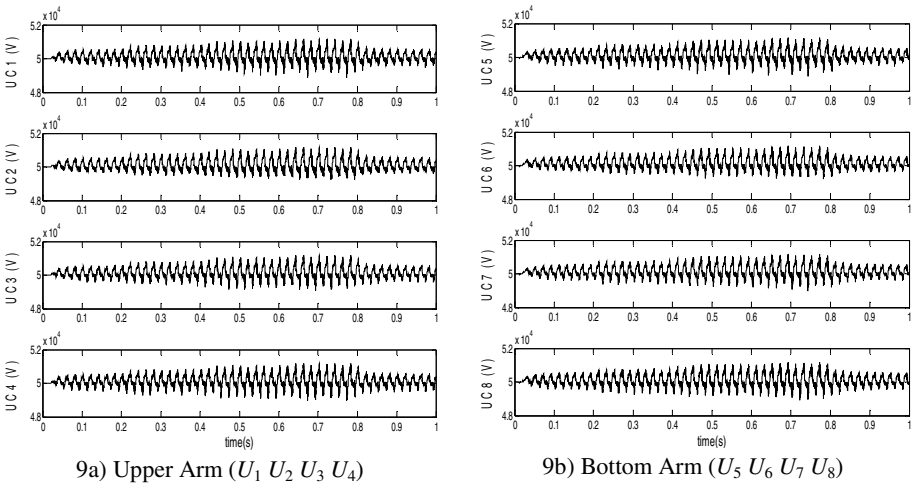

9a) Upper Arm (U_1 U_2 U_3 U_4)   9b) Bottom Arm (U_5 U_6 U_7 U_8)

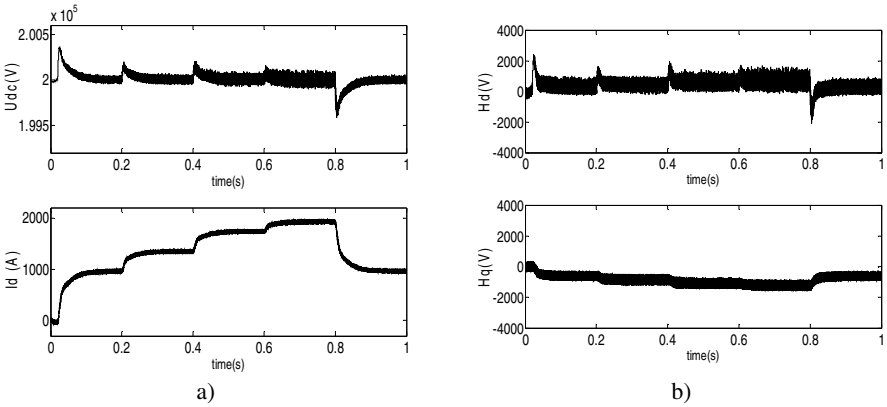**Fig. 9.** Simulation results showing balanced capacitor voltages in arm 1 of $3M^3C$

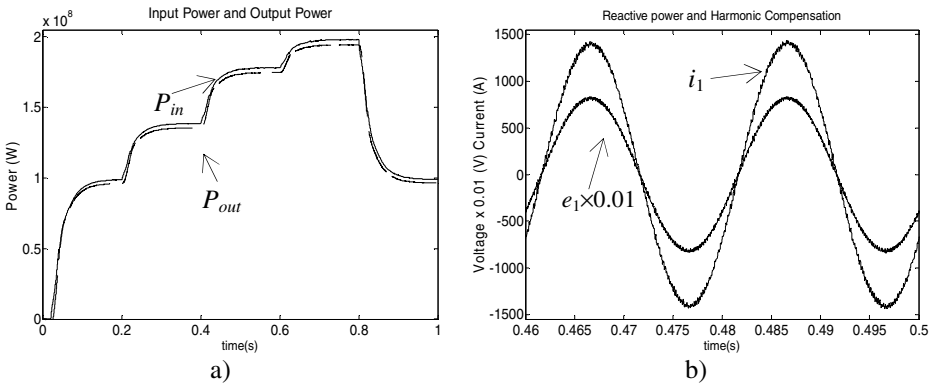**Fig. 10.** Simulation results of linear control: a) U_{dc} voltage and I_d b) H_d and H_q

Fig. 11. Simulation results a) Output and input powers b) Current and voltage×0.01 in phase1
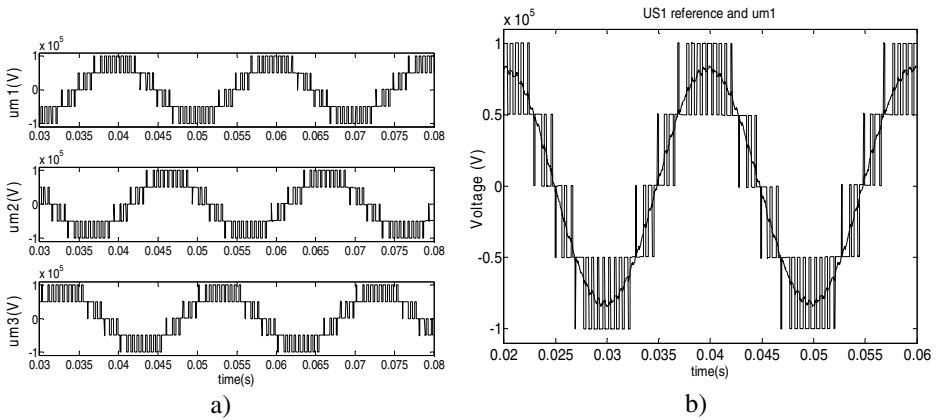

Fig. 12. Simulation results a) Three-phase ac output voltages b) U_{S1ref} and u_{m1}

Fig. 10a shows the linear control of the U_{dc} voltage (top left waveform) and the 2nd waveform presents the I_d control. The 1st waveform (top right) of Fig. 10b shows the H_d component and the 2nd waveform presents H_q component. Fig. 11a presents input and output power figures to show the high efficiency of this power converter ($\approx$98%). Reactive power compensation is observed in Fig. 11b, in which the phase angle between current (in line 1) and voltage ($Us\times0.01$) (in phase 1) is zero. Fig. 12a show the three-phase converter ac output voltages (u_{m1}, u_{m2} and u_{m3}).   Fig. 12b presents converter ac output voltage in phase 1 and sinusoidal output voltage reference U_{S1ref}.

6   Conclusions

This paper has presented modular multilevel converter for connecting an offshore wind park to the inshore ac power grid network (HVDC-VSC). The three-phase modular multilevel Marx converter ($3M^3C$) has five levels in each arm.

The multilevel converter was built with modular MC cells that can be used to build multilevel converter with high number of levels. The capacitor voltage equalization is obtained with a strategy (*Vector Decision* algorithm) that does not need to measure the capacitor voltages. The dc link capacitor voltage control was designed using a linear controller. Sigma-delta modulators were used to obtain the converter ac output voltages, and average current control was used for power flow control, harmonics and reactive power compensation. Presented simulations have shown the effectiveness of the proposed strategy.

References

1. Adam, G.P., Anaya-Lara, O.G., Burt, M.J.: Comparison between Two VSC-HVDC Transmission Systems Technologies: modular and Neutral Point Clamped Multilevel Converter. In: 35th Annual Conference of the IEEE Industrial Electronics Society – IECON Porto, Portugal (2009)
2. Encarnação, L., Silva, J.F., Pinto, S.F., Redondo, L.M.: A New Modular Marx Derived Multilevel Converter. In: 2nd Doctoral Conference on Computing Electrical and Industrial Systems – DoCEIS Costa da Caparica, Portugal (2011)
3. Lesnicar, A., Maruardt, R.: An Innovative Modular Multilevel Converter Topology Suitable for a Wide Power Range. In: IEEE Power Tech. Conference, Bologna, Italy (2003)
4. Redondo, L.M., Fernando, J.F.: Repetitive High-Voltage Solid-State Marx Modulator Design for Various Load Conditions. IEEE Transactions on Plasma Science 37(8), 1632–1637 (2009)
5. Franquelo, L.G., Rodríguez, J., Leon, J.I., Kouro, S.: The age of multilevel converters arrives. IEEE Industrial Electronics Magazine 2(2), 28–39 (2008)
6. Encarnação, L., Silva, J.F.: Reactive Power Compensation Using Sliding-Mode Controlled Three Phase Multilevel Converters. In: 12th International Conference on Harmonics and Quality of Power – ICHQP Cascais, Portugal (2006)
7. Hagiwara, M., Akagi, H.: PWM Control and Experiment of Modular Multilevel Converters. In: IEEE Power Electronic Specialist Conference, Rhodes, pp. 154–161 (2008)
8. Silva, J.F., Pinto, S.F.: Control Methods for Switching Power Converters. In: Rashid, M.H. (ed.) Power Electronics Handbook, 2nd edn., USA, ch. 34, pp. 935–998, 1172. Academic Press, Elsevier (2007) ISBN 13:978-0-12- 088479-7, ISBN 10:0-12-088479-8
9. Encarnação, L., Silva, J.F.: Sliding Condition Based Sliding Mode Modulators for Multilevel Power Converters. In: 35th Annual Conference of the IEEE Industrial Electronics Society – IECON Porto, Portugal (2009)